NeuroImage 133 (2016) 163–175

Contents lists available at ScienceDirect

NeuroImage

journal homepage: www.elsevier.com/locate/ynimg

Lines of Baillarger in vivo and ex vivo: Myelin contrast across lamina at 7 T MRI and histology

Alessio Fracasso [a,b,c,*], Susanne J. van Veluw [d], Fredy Visser [b,e], Peter R. Luijten [b], Wim Spliet [f], Jaco J.M. Zwanenburg [b], Serge O. Dumoulin [a,c,1], Natalia Petridou [b,1]

[a] Experimental Psychology, Helmholtz institute, Utrecht University, Utrecht, Netherlands
[b] Radiology, Imaging Division, University Medical Center, Utrecht, Netherlands
[c] Spinoza Centre for Neuroimaging, Amsterdam, Netherlands
[d] Neurology, Brain Center Rudolf Magnus, University Medical Center, Utrecht, Netherlands
[e] Philips Medical Systems, Best, Netherlands
[f] Pathology, University Medical Center Utrecht, Utrecht, The Netherlands

ARTICLE INFO

Article history:
Received 3 December 2015
Accepted 26 February 2016
Available online 3 March 2016

ABSTRACT

The human cerebral cortex is characterized by a number of features that are not uniformly distributed, such as the presence of multiple cytoarchitectonic elements and of myelinated layers running tangentially to the cortex surface. The presence and absence of these features are the basis of the parcellation of the cerebral cortex in several areas. A number of areas show myelin increases localized within the cortex, e.g., the stria of Gennari located in layer IV of the primary visual cortex. Sub-millimeter MRI can resolve myelin variations across the human cortex and may allow in vivo parcellation of these brain areas. Here, we image within-area myelination. We modified a T1-weighted (T1-w) MPRAGE sequence to enhance myelin visualization within the cortex. First, we acquired images from an ex vivo sample, and compared MRI laminar profiles from calcarine (corresponding to primary visual cortex) and extra-calcarine areas with histology sections from the same locations. Laminar profiles between myelin stained sections and the T1-w images were similar both in calcarine as well as extra-calcarine cortex. In calcarine cortex, the profile reveals the stria of Gennari. In extra-calcarine cortex, a similar profile exists which we suggest corresponds to the lines of Baillarger. Next, we adapted the same sequence to image within-area myelination in vivo.
Also in in vivo data, we discriminated similar laminar profiles in calcarine and extra-calcarine cortex, extending into parietal and frontal lobes. We argue that this myelin pattern outside the calcarine cortex represents the lines of Baillarger.

Introduction

The human cerebral cortex is characterized by laminar features that are not distributed uniformly across its extent. Differences in local cortical thickness, the presence of multiple myelinated layers, and differences in cytoarchitecture make it possible to recognize different areas within the cerebral cortex (myeloarchitectonics: Vogt, 1903 and cytoarchitectonics: Brodmann, 1909).

Since the beginning of the twentieth century, these features are the basis for neuroanatomical studies of the cortex and the efforts for its parcellation, in order to link local structure to function (Vogt, 1903; von Economo and Koskinas, 1925; for a review, see Geyer and Turner, 2013; Nieuwenhuys, 2013; for a meta-analysis of data from the Vogt–Vogt school see Nieuwenhuys et al., 2014).

Modern neuroimaging methods allow the investigation of the functional and structural organization of the human cerebral cortex, in vivo. Recent advances have been particularly successful in visualizing myelination patterns in vivo across the cortex. These myelination patterns are used to identify a large number of cortical areas that can match probabilistic cytoarchitectonic atlases and retinotopic maps (Fischl et al., 2008; Hinds et al., 2008; Bock et al., 2013; Glasser and Van Essen, 2011; Marques and Gruetter, 2013; Sereno et al., 2013; Sánchez-Panchuelo et al., 2012, 2014; Lutti et al., 2014; Dinse et al., 2015; Tardif et al., 2015).

Some studies visualized detailed myelination patterns within the human primary visual cortex, visualizing the stria of Gennari (Barbier et al., 2002; Bridge et al., 2005; Eickhoff et al., 2005; Trampel et al., 2011), as well as intra-cortical details in locations outside primary visual cortex (Sánchez-Panchuelo et al., 2012), and in motion-sensitive area V5 (Walters et al., 2003).

* Corresponding author at: Experimental Psychology, Helmholtz institute, Utrecht University, Heidelberglaan 1, Room H0.33, 3584 CS Utrecht, Netherlands.
E-mail address: alessio.fracasso@gmail.com (A. Fracasso).
[1] Equal contribution.

http://dx.doi.org/10.1016/j.neuroimage.2016.02.072
1053-8119/

The stria of Gennari is a band of highly myelinated fibers that runs tangentially to the gray matter surface in primary visual cortex, at the level of layer IV (Gennari, 1782). Due to its presence, the primary visual cortex is also known as the striate cortex. This structure is visible to the naked eye on macroscopic examination of the brain and represents a special case of the outer band of the lines of Baillarger (Baillarger, 1840). The lines of Baillarger consist of two bundles of myelinated fibers, located in the internal granular layer of layer IV and internal pyramidal layer of layer V. At a microscopic level, the lines of Baillarger can be found throughout the cortex (Baillarger, 1840). However, these lines have not been visualized in vivo in humans, except visual area V5/MT (Walters et al., 2003), whereas they have been visualized on ex vivo samples (Waehnert et al., 2014). This is probably due to the lower contrast and smaller thickness that characterize this particular dual-band structure, as compared to the stria of Gennari.

Here we aim to visualize myelin variations within the human cortex combining in vivo, ex vivo, and histological measurements.

We extended a T1-weighted (T1-w) magnetization prepared rapid acquisition gradient recalled echo (MPRAGE) sequence (Bock et al., 2009) to optimize contrast between low and high myelin content within human cortex. We compared high-resolution MRI intensity profiles along cortical thickness (laminar profiles) from calcarine and extra-calcarine areas from an ex vivo sample with corresponding histology sections from the same locations. In calcarine cortex, the profile reveals the stria of Gennari. In extra-calcarine cortex, a similar profile exists which we suggest corresponds to the lines of Baillarger. Next, we adapted the same sequence to image within-area myelination in vivo. Also, in in vivo data, we discriminated similar laminar profiles in calcarine and extra-calcarine cortex extending into parietal and frontal lobes. We suggest that this myelin pattern outside the calcarine cortex represents the lines of Baillarger.

Methods

Ex vivo imaging

Formalin-fixed brain samples were obtained from one human subject (54-year-old female) who had undergone autopsy in our hospital (University Medical Center Utrecht, UMCU) to establish cause of death (Fig. 1A). The subject had no known (history of) cerebral disease. The use of this tissue was in accordance with local regulations and approved by the medical ethics committee of the UMCU. The arachnoid was removed prior to scanning. The slices were placed in a plastic formalin-filled container and scanned overnight. Images were acquired using a 7 Tesla MR system (Philips Healthcare, Cleveland, OH, USA; gradient strength: 40 mTm, slew rate: 200 T/m/s) with a volume transmit and 32-channel receive head coil (Nova Medical, Wilmington, MA, USA).

Images were acquired with a 3D T1-w MPRAGE sequence optimized for ex vivo imaging, accounting for the changed T1 relaxation time constant of brain tissue after formalin fixation. The inversion delay (TI) was adjusted such that the gray matter (GM) signal was just above the null point, while the time delay (TD) between inversion pulses was chosen long enough to reduce the difference in longitudinal magnetization between white and gray matter prior to the inversion pulse. Thus, high contrast between white and gray matter was obtained, yielding optimal contrast between gray matter with high myelin content ("white matter like") and gray matter with low myelin content. The following parameters were used: TR/TE: 7.7/3.5 ms, flip angle: 8 degrees, adiabatic inversion, TI: 280 ms, TD: 2 s, resolution $400 \times 400 \times 400$ μm^3, 80 slices, bandwidth 202 Hz/pixel, no acceleration, scan duration approximately 1 h and 9 min. A proton density (PD) scan was acquired for subsequent correction of B1 field inhomogeneity as follows: 3D turbo-field echo, TR/TE: 9/2 ms, FOV: $140 \times 132 \times 40$, flip angle = 1 degree, voxel size: $1 \times 1 \times 2$ mm^3, 40 coronal slices, BW: 506 Hz/px, no acceleration, scan duration = 33 s. Very high-resolution T2*-weighted (T2*-w) w gradient echo images were acquired as an anatomical reference (3D T2*-w gradient echo TR/TE: 75/20 ms, flip angle 25 degrees, bandwidth 53 Hz/pixel, resolution $180 \times 180 \times 180$ μm^3, 278 slices, no acceleration, scan duration approximately 5 h). Examples of the T1*-w and T2*-w images are shown in Fig. 1B and C. T2*-w images, particularly phase images, show excellent contrast for the stria of Gennari (Duyn et al., 2007). Here, both magnitude and phase images were reconstructed but phase images had to be discarded because of susceptibility artifacts caused by air bubbles trapped in the sample. Therefore, we used the magnitude images for anatomical reference.

Histology

After imaging, representative areas from the calcarine cortex and areas from extra-calcarine cortex were excised and subjected to standard histological analysis. The tissue was dehydrated and embedded in paraffin. 4-μm thick serial sections were cut using a microtome, and adjacent sections were stained with Luxol fast blue–periodic acid Schiff (LP) for the visualization/identification of myelin. Obtained sections were studied using a microscope, with a camera mounted on top of the microscope. For further analysis, pictures were taken from histological samples (resolution: 1280×1024).

In vivo imaging

Four males participated in the in vivo experiment occipital pole acquisition, and five males participated in the in vivo experiment whole-brain acquisition (age range 25–39 years). All experimental procedures were conducted in accordance with the 1964 Declaration of Helsinki (most recently amended in 2008, Seoul), and approved by the ethics

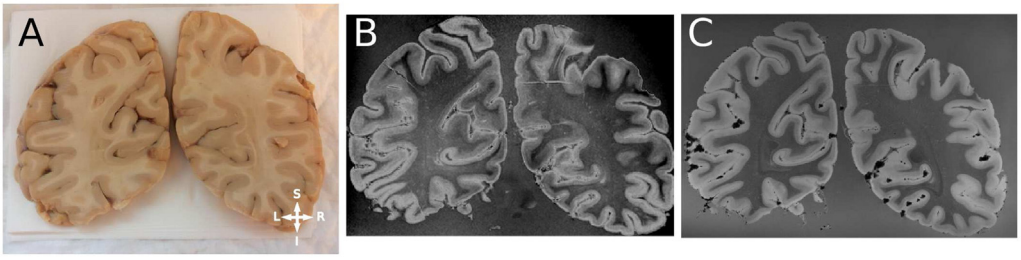

Fig. 1. Panel A, for each location the volume was manually segmented, delineating WM and the CSF borders. Panel B, WM mesh and CSF mesh, the valid normals (normals that intersect the CSF mesh, blue arrows) are drawn over the WM mesh. Single profiles were obtained by interpolating (via nearest neighbor interpolation) the volume along the valid normals until reaching the CSF mesh in 100 steps. Panel C, all the profiles for each location were averaged together (only 13 points are reported, the complete profile consisted of 100 points). Panel D, data from the average profile was smoothed to low-pass the signal. Green arrow represents the first positive to negative zero-crossing point of the first derivative, continuous and dotted red lines represent the median first negative to positive zero-crossing point from the bootstrapping procedure, and 95%CI, respectively. The error bars indicate the standard deviation over all profiles.

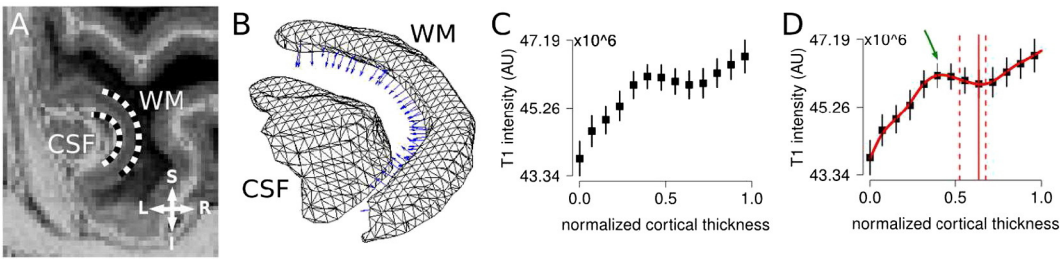

Fig. 2. Panel A, sample of one of the ex vivo human brain slices that underwent scanning. Panel B, T1-w image (please note that contrast is inverted for visualization purposes) acquired at 0.4 mm isotropic resolution. Panel C, representative image of the T2*-w data acquired at 0.18 mm isotropic resolution.

committee of the UMCU. Images were obtained using a similar T1-w MPRAGE sequence as used for the ex vivo scan, optimized for in vivo imaging. A strong contrast between gray and white matter was obtained with TD = 6 s (approximately 3 times the T1 of GM, allowing full recovery of both GM and white matter (WM) prior to inversion) and TI = 1200 ms (yielding GM signal just above zero). At this TI and TD, cerebrospinal fluid (CSF) appears bright in the reconstructed magnitude images (Fig. 5). Occipital and whole-brain images were acquired per subject, as described below. A PD scan centered on the occipital and whole-brain field-of-view (FOV), respectively, was acquired for subsequent correction of B1 field inhomogeneities and for correction of the intensity inhomogeneity due to the sensitivity profiles of the receive coils. Head-motion was limited by foam padding.

Occipital images

The FOV was centered on the occipital pole. Acquisition parameters were TD/TI: 6000/1200 ms, adiabatic inversion, TR/TE: 8/4 ms, flip angle: 8 degrees, voxel size: 500 × 500 × 500 μm^3, FOV: 140 × 140 × 30 mm^3, 60 coronal slices, bandwidth 202 Hz/px, number of excitations per inversion: 275, linear readout, and no acceleration. Scan duration was ~7.5 min, 6 repeated scans were acquired per participant. This protocol was adopted to increase the signal-to-noise ratio (which would be compromised with the use of accelerated imaging) at the cost of scan time duration. PD scan parameters: 3D turbo-field echo, TR/TE: 9/2 ms, FOV: 140 × 140 × 30 mm, flip angle = 1 degree, voxel size: 1 × 1 × 1 mm^3, 30 coronal slices, BW: 506 Hz/px, no acceleration, scan duration = 26 s.

Whole-brain images

The whole-brain protocol included acceleration to investigate the feasibility of the technique within clinically acceptable scan times. Whole-brain coverage was obtained with the following parameters: TD/TI: 6000/1200 ms, adiabatic inversion, TR/TE: 8/3 ms, flip angle: 8 degrees, voxel size = 500 × 500 × 500 μm^3, FOV: 250 × 250 × 180 mm^3, 360 sagittal slices, bandwidth 201 Hz/px, number of excitations per inversion: 300, linear readout, acceleration using SENSE: 2.5 (anterior–posterior) × 2.5(right–left). Additionally, we used an optimized linear sampling scheme over ky and kz provided by the vendor software (termed Free factor), effectively allowing a high number of excitations per inversion in combination with an elliptical k-space shutter. Scan duration was 7.5 min (4–5 repetitions were acquired for each participant, scan duration without the use of Free factor would be ~15 min). PD scan parameters: 3D turbo-field echo, TR/TE: 6/3 ms, FOV: 250 × 250 × 180 mm, voxel size: 1 × 1 × 1 mm^3, flip angle 1 degree, 180 sagittal slices, BW: 253 Hz/px, SENSE: 1.8 (anterior–posterior) × 1.8(right–left), scan duration 48 s. The same sequence was used to acquire the data for two participants with a different resolution (voxel size = 600 × 600 × 600 μm^3) with all other parameters being the same, as a control for the presence of Gibbs ringing (truncation artifacts).

Preprocessing

Ex vivo

The T2*-w images were used for GM and WM segmentation and the segmentation was subsequently applied on the T1-w images. Segmentation of the images was performed manually (see below: *Laminar analisis*). T2*-w images (and segmentation images) were interpolated to 400 μm^3 voxels by means of nearest interpolation, to match the T1-w scan resolution and manually realigned to the T1-w scan using Slicer (Fedorov et al., 2012). Please note that the contrast is inverted T1-w images to match the contrast on the histology samples. The correspondence between histology and ex vivo MRI was obtained by visually inspecting the images.

In vivo

In vivo occipital and whole-brain T1-w images were corrected for head movement between scan acquisitions using the 3dAllineate function in AFNI (http://afni.nimh.nih.gov), using 6 degrees of freedom and imposing wsinc5 as the last interpolation step. After motion correction, images of the same FOV were averaged together to increase SNR. PD images were resampled to the corresponding T1-w space and blurred with a Gaussian smoothing kernel (full width half max = 12 mm). T1-w images were divided by the blurred PD images of the corresponding FOV. Please note that the contrast is inverted T1-w images to match the contrast on the histology samples.

Location selection

Ex vivo

Five different locations were sampled for histological analysis: left/right calcarine cortex, a location dorsal to the left calcarine, and a left/right location ventral to the calcarine cortex. The same locations were selected on the T2*-w and T1-w images.

In vivo

Four locations were selected from the occipital T1-w images for each participant: two in the calcarine cortex and two in extra-calcarine locations. On the whole-brain T1-w images, we selected 4 similar locations in the occipital, parietal, and frontal lobes for each hemisphere per participant (total of 12 separate locations for each participant). Selection of extra-calcarine locations in the cortex was motivated by visual observation of a striated appearance within the cortex.

Laminar analysis

For each location, the volume was manually segmented using Slicer (Fedorov et al., 2012), delineating WM and the CSF (Fig. 2A). The segmented WM and CSF were smoothed with a Gaussian kernel (std = 0.8 voxels). The faces and vertices of the WM and CSF meshes were extracted from the isosurface of the volume (using the MATLAB function isosurface). The normals of the white mesh were computed and

grown until they intersected the CSF mesh. Only the normals that intersected the CSF mesh were kept for subsequent analysis (valid normals), all the other normals were not analyzed further (Fig. 2B, blue arrows). Individual profiles were obtained by interpolating (via nearest neighbor interpolation) the volume along the valid normals until reaching the CSF mesh in 100 steps.

The Euclidean distance with respect to GM-WM border was computed (Ress et al., 2007 equidistance approach). Waehnert et al. (2014) showed that an equivolume approach in estimating layer 4 location outperformed the equidistance approach for extremely high acquisition resolutions (~0.1 mm isotropic). However, they also showed that the equivolume and equidistance approaches were indistinguishable at relatively lower resolutions (0.5 mm isotropic).

For each location, a variable number of individual profiles was obtained, ranging from 25 to 45 profiles. All the profiles were averaged together (Fig. 2C, only 13 points are reported, the complete profile consisted of 100 points). Then, the average profile was smoothed using the R software (http://www.R-project.org) implementation of cubic

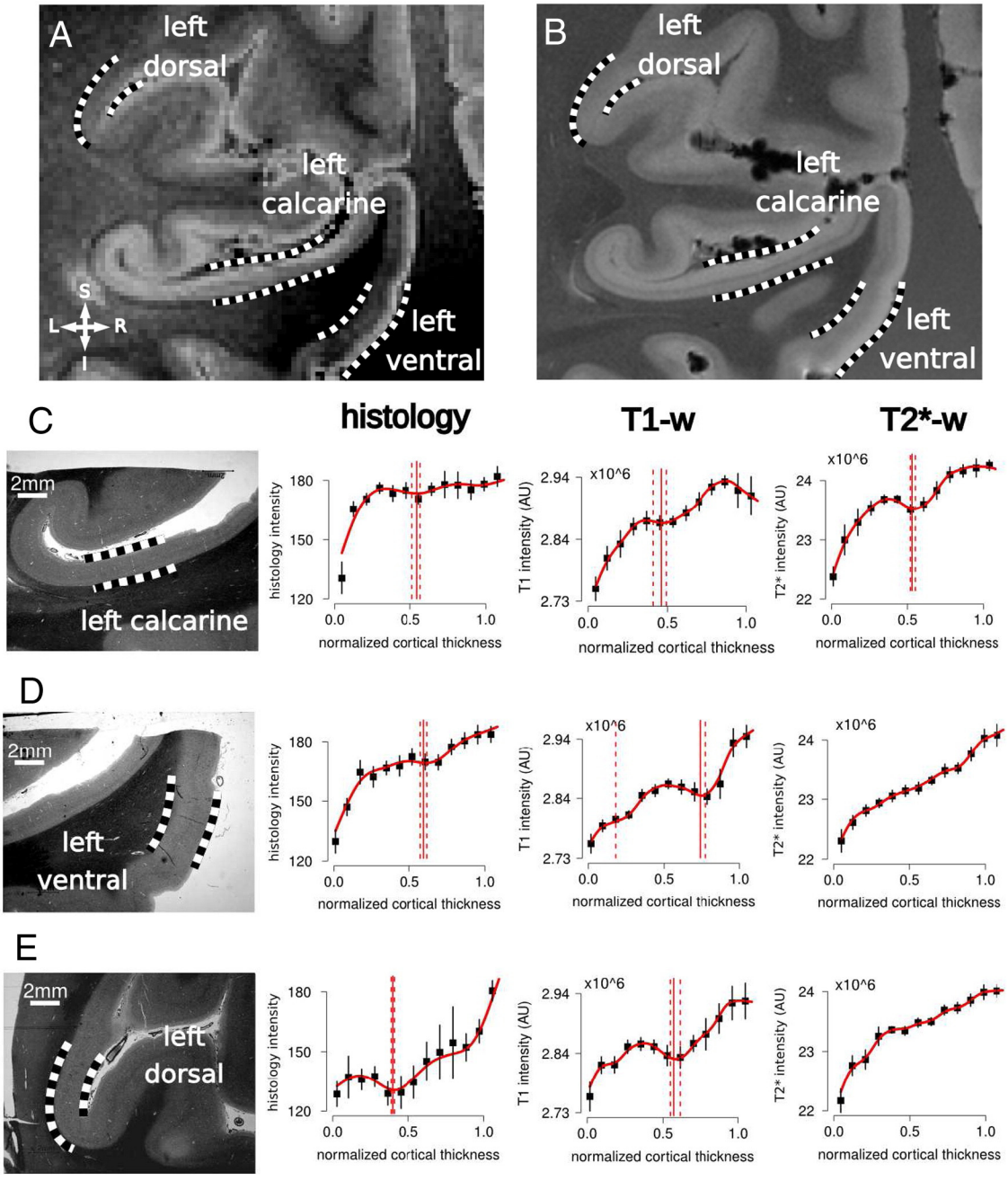

Fig. 3. Panel A, zoomed view of the ex vivo T1-w data, left hemisphere, and the selected locations that underwent laminar analysis: left calcarine, left dorsal location (with respect to calcarine), and left ventral location (with respect to calcarine). Panel B, zoomed view of the T2*-w data, left hemisphere (0.18 mm isotropic), and the selected locations that underwent laminar analysis. Myelin stain images taken from the above selected locations and the corresponding laminar profiles extracted from histology, T1-w data and T2*-w data are listed in rows C to E. Row C, left calcarine location. Row D, left ventral location (with respect to the calcarine). Row E, left dorsal location (with respect to the calcarine). Plots show averaged laminar profiles per location from the GM/WM border (0 on the x-axis) to the GM/CSF surface (1 on the x-axis). The error bars indicate standard deviation over all profiles for each location. A red dotted line was drawn if an hypo-intense band was identified in more than 75% of the bootstrapped profiles on a single location (see 'Laminar analysis'). Significant hypo-intense bands were found in the histology and T1-w intensity profiles. For the T2*-w intensity profiles, a hypo-intense band could be identified for the calcarine cortex, but not on locations ventral and dorsal with respect to the calcarine. Example of additional high-resolution histology images can be found in Fracasso et al., 2016, figure 16.

spline fit with 0.55 as a smoothing parameter (Fig. 2D). The smoothing step was incorporated to low-pass the signal, in order to find a stable zero-crossing point in the first derivative of the profile, see below.

An estimate of a change in profile intensity along the average profile was derived by means of a bootstrapping procedure (2000 repetitions with replacement). A change in the profile intensity was defined as the first negative-to-positive zero-crossing point of the first derivative of the smoothed profile, extracted for each bootstrapped iteration, if it existed (hypo-intense band). For each iteration, we extracted also the first positive to negative zero-crossing point of the first derivative, if it existed, giving an index of where the hypo-intense band started along the profile (see green arrow, Fig. 2D).

For any given location, we assessed whether the proportion of bootstrapped samples where a hypo-intense band was identified statistically exceeded 75%, using the test of given proportions. Multiple tests were corrected using Bonferroni correction. In case we could reject the null hypothesis that the proportion was smaller than or equal to 75%, a reliable hypo-intense band in profile intensity was identified for that specific location.

For any given location we assessed the amplitude of the hypo-intense band by subtracting the profile intensity at start of the hypo-intense band (see green arrow, Fig. 2D) from the profile intensity at the minimum of the hypo-intense band (red continuous line, Fig. 2D).

Intensity profiles inside the white matter, control profiles

Gibbs ringing consists of multiple, parallel bands of alternating bright and dark signal from a high contrast border, due to k-space truncation. Gibbs ringing would manifest on either side of a high contrast border (thus inside GM and also inside WM). For each participant, we measured T1-w intensity profiles from 4 locations for the whole-brain scan, sampling intensity profiles inside WM towards GM. We analyzed the result for the presence of a hypo-intense band along the profiles (see Fig. 10). Differences in amplitude of the hypo-intense band between different locations were assessed via within-participant ANOVA, and Bonferroni corrected t-test for post-hoc analysis.

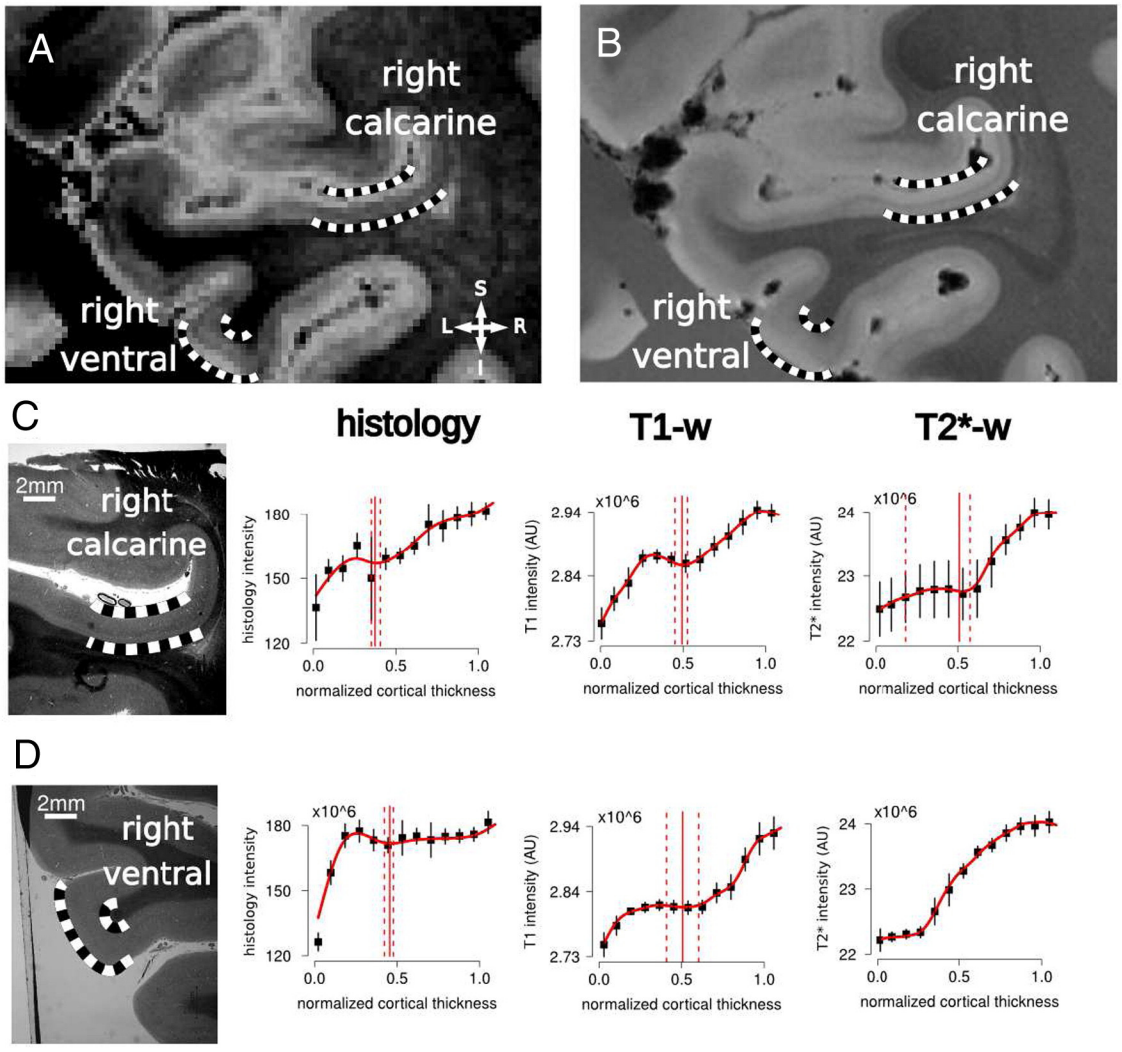

Fig. 4. Panel A, zoomed view of the ex vivo T1-w data, right hemisphere, and the selected locations: right calcarine, right ventral location (with respect to calcarine). Panel B, zoomed-view of the T2*-w data, right hemisphere (0.18 mm isotropic). Myelin stain images taken from the above locations and the corresponding laminar profiles extracted from histology, T1-w data and T2*-w data are listed in rows C and D. Row C, right calcarine location. Row D, right ventral location (with respect to the calcarine). Plots represent laminar profiles from GM/WM (0 on the x-axis) to GM/CSF surface (1 on the x-axis), the error bars indicate standard deviation over all profiles. A red dotted line was drawn if a hypo-intense band was identified in more than 75% of the bootstrapped profiles on a single area (see 'Laminar analysis'). Hypo-intense bands were found in the histology and T1-w intensity profiles. For the T2*-w intensity profiles, a hypo-intense band could be identified for the calcarine cortex, but not on the location ventral with respect to the calcarine. Example of additional high resolution histology images can be found in Fracasso et al. 2016, figure 16.

Within-scan noise level estimates

To assess whether within-scan motion corrupted the image quality, we compared the noise level estimates along the phase encoding direction. For each participant and acquired whole-brain volume, we arbitrarily defined 10 ROIs (10 cubic voxels) on posterior locations and 10 ROIs on anterior locations (outside the brain). For each ROI, we obtained a noise estimate by computing the average T1-w signal divided by the standard deviation of the T1-w across all the voxels in the ROI. Values on the anterior and posterior ROIs across participants were compared by means of two-sample t test.

In vivo data, surface analysis

For the surface analysis on whole-brain data, images were downsampled to 1 mm isotropic resolution, using nearest neighbor interpolation. In this way, data were compatible with FreeSurfer pipeline (http://freesurfer.net/), and cortical surfaces were reconstructed. The surface analysis on the whole-brain images was performed in the following way: image intensity was sampled halfway the cortical thickness, based on the FreeSurfer cortical thickness estimate. The global mean intensity was subtracted from the intensity value distribution and corrected for local curvature by means of linear regression (Sereno et al., 2013).

Results

Histology

Histological laminar profiles showed a characteristic pattern, a hypo-intense band in image intensity, located at the middle of cortical thickness was found for all selected locations, i.e. calcarine (Figs. 3C and 4C), and extra-calcarine (Figs. 3D, E and 4D). In calcarine cortex, the location of the hypo-intense band corresponded to the highly myelinated stria of Gennari, the structure that identifies primary visual cortex. A similar hypo-intense band located at the middle of cortical

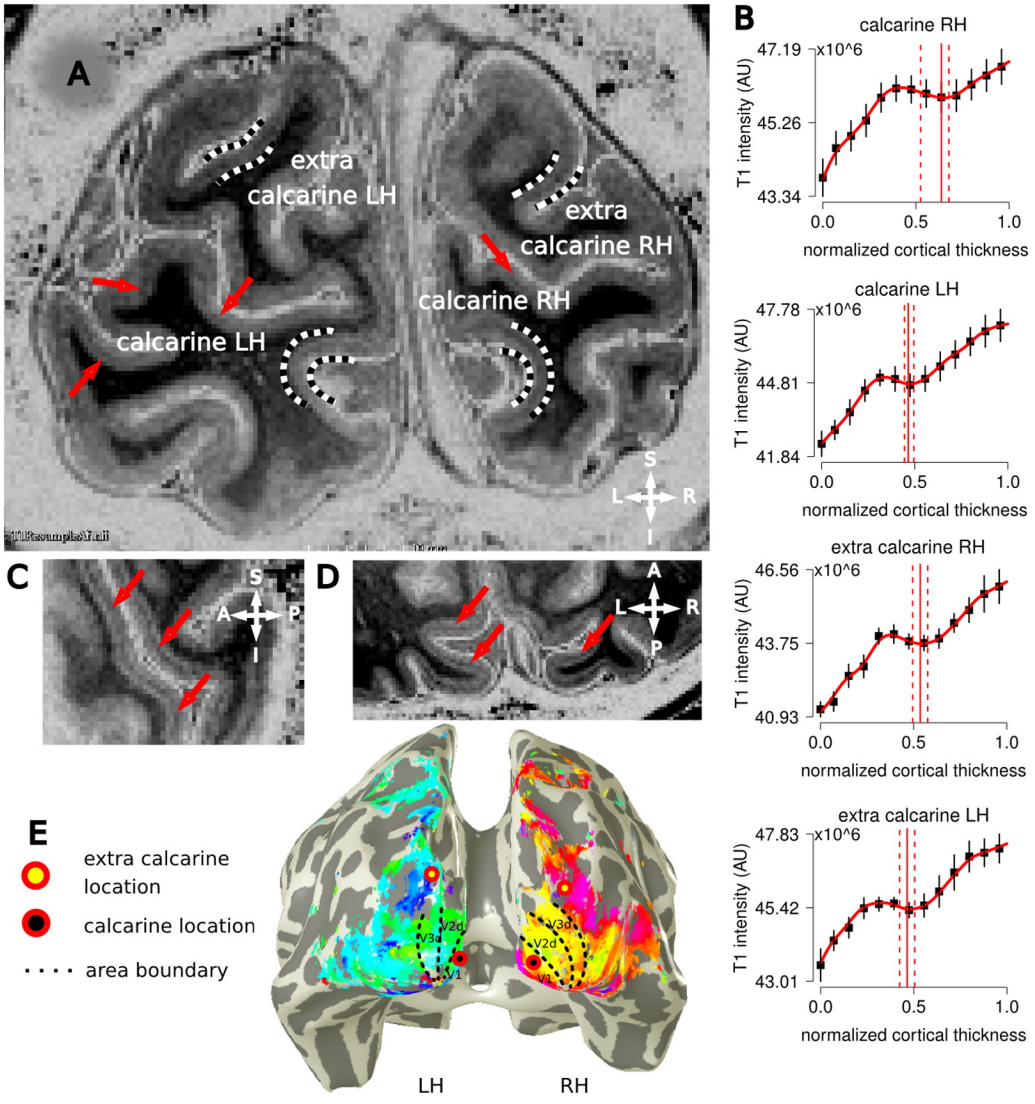

Fig. 5. Panel A, coronal slice, in vivo T1-w image for one participant (P1). Locations in the calcarine cortex and extra-calcarine cortex are indicated in the image (black white dotted lines). Red arrows point to other locations where hypo-intense band is visible around the middle of cortical thickness. Panel B, Laminar profiles are reported from the GM/WM border (0 on the x-axis) to the GM/CSF surface (1 on the x-axis) for each location, error bars indicate the standard deviation over all profiles for each location, vertical red lines in represent median and bootstrapped 95% CI of hypo-intense band location. A hypo-intense band in T1-w images was identified in more than 75% of the bootstrapped profiles (see 'Laminar Analysis') in calcarine and extra-calcarine locations, see Fracasso et al., 2016 for data from the 3 other participants. Panel C, sagittal view. Panel D, axial view, centered on the calcarine. Panel E, early visual area retinotopic maps for participant 1, superimposed on a reconstructed whole-brain 3D mesh. Areas V1 to V3 as well as V3A and V3B are reported. Black dots with a red surround represent calcarine locations projected to the mesh surface, yellow dots with a red surround represent extra-calcarine locations projected to the mesh surface. Extra-calcarine locations are well outside the functionally defined area V1.

thickness was found also moving dorsally and ventrally with respect to the calcarine cortex.

Ex vivo

T1-w and T2*-w intensity laminar profiles from the calcarine cortex of the ex vivo sample showed a monotonic increase towards the GM/CSF surface, similar to histology. A hypo-intense band in T1-w and T2*-w intensity was identified around the middle of the cortical thickness corresponding to the location of the highly myelinated stria of Gennari. Moving dorsally and ventrally with respect to the calcarine cortex, a similar hypo-intense band, located around the middle of the cortical thickness, was identified for the T1-w intensity profiles, but it was not observed along the T2*-w intensity profiles (see Fig. 3, rows C, D, and E; Fig. 4, rows C and D, T1-w and T2*-w profiles).

In vivo occipital T1-w images and laminar profiles

Analysis of the occipital T1-w in vivo data showed a hypo-intense band in the middle of the cortical thickness similar to the ex vivo data. For the calcarine cortex, this feature can be related to the stria of Gennari (Fig. 5A,B). Moreover, extra-calcarine areas also showed a similar hypo-intense band in T1-w intensity in the middle of the cortical thickness (Fig. 5A). The location of these areas is not compatible with the calcarine cortex and is well outside the range of primary visual cortex (Fig. 5E, for details about visual field mapping see Fracasso et al., 2016, figures 2–5).

The hypo-intense band in T1-w images located around the middle of the cortical thickness was consistently observed across all 4 participants for the occipital in vivo T1-w scan (Fig. 6, see Fracasso et al., 2016, figures 2–5 for retinotopic mapping results and intensity profiles of all participants from calcarine and extra calcarine areas).

Hypo-intense band amplitude was compared between calcarine and extra-calcarine locations by means of a paired samples t-test. The test showed a difference between calcarine and extra-calcarine locations ($T(7) = 4.46$, $p < 0.05$). A larger amplitude of the hypo-intense band was observed for the former compared to latter locations.

The largest motion detected across multiple repetitions for each participant is reported in Fracasso et al., 2016, table 1, estimated motion parameters across participants and scans ranged from a minimum of 0.55 mm to a maximum of 2.8 mm.

In vivo whole-brain T1-w surface map

The surface analysis of the whole-brain images revealed cortical myelination maps consistent with previous reports (Glasser and Van Essen, 2011; Sereno et al., 2013). After correcting for local curvature, a number of cortical locations showed increased myelination, located at the level of the calcarine sulcus, central, and post-central sulcus, the superior temporal sulcus and middle temporal cortex (compatible with motion-sensitive area MT). Fig. 7 shows the results for one participant. Results were similar for all participants.

In vivo whole-brain T1-w images and laminar profiles

Fig. 8 shows example coronal, axial and sagittal slices for one participant (P2, similar results were found for all participants, the complete dataset with the 5 participants can be found on Fracasso et al., 2016).

T1-w profiles were also obtained from the whole-brain T1-w in vivo scans. A hypo-intense band on T1-w images around the middle of cortical thickness was detected for locations in occipital cortex (Fig. 9, column A) and parietal cortex (Fig. 9, column B). Importantly, this hypo-intense band was also detected for the locations in frontal cortex (Fig. 9, column C), a region typically not associated with increased within-area myelination. Results were similar for all participants (data from the other 4 participants can be found in Fracasso et al., 2016, Figures 6–15).

The largest motion detected across multiple repetitions for each participant is reported in Fracasso et al., 2016, Table 1, estimated motion parameters across participants and scans ranged from a minimum of 0.45 mm to a maximum of 1.5 mm.

Results of the within-participant ANOVA for the T1-w images showed a main effect of location where the profiles where extracted

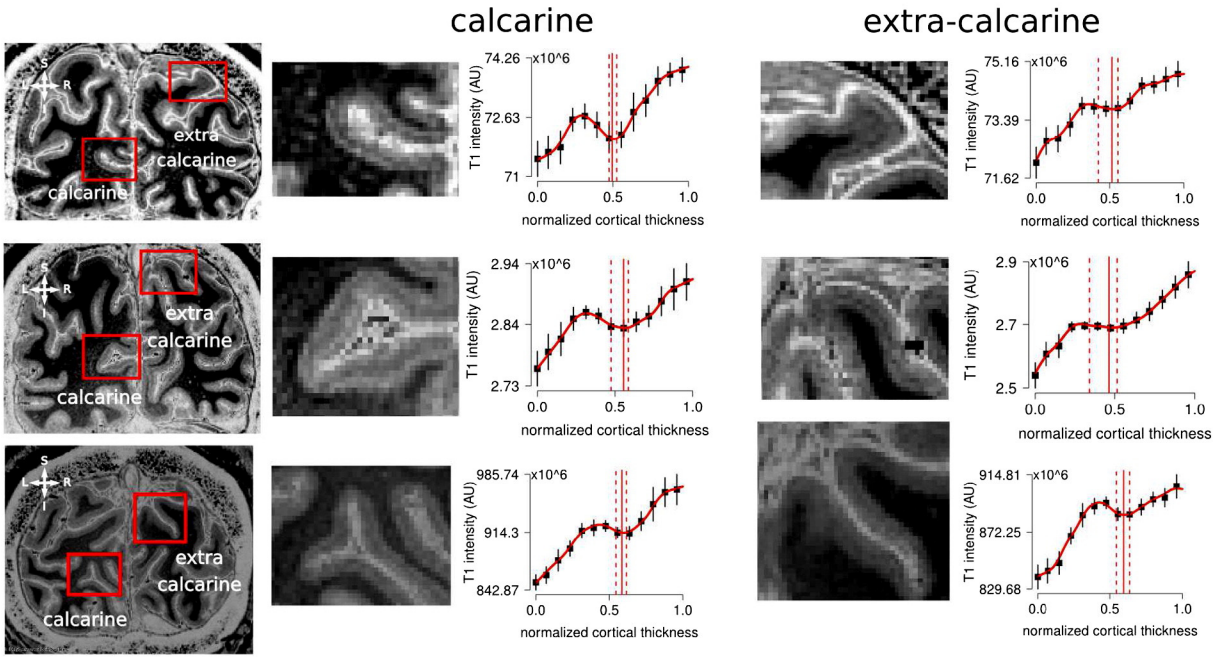

Fig. 6. in vivo T1-w images and profiles for participants 2–4 (separate rows), for calcarine and extra-calcarine locations. Left column: Example occipital T1-w images. Red squares on the images mark the selected calcarine and extra-calcarine locations. These locations are shown enlarged in the middle and right columns respectively, with the corresponding laminar profile. Laminar profiles are reported from the GM/WM border (0 on the x-axis) to the GM/CSF surface (1 on the x-axis) for each location. Error bars indicate standard deviation over all profiles for each location, vertical red lines in graphs represent median and bootstrapped 95% CI of hypo-intense band location. Consistent hypo-intense bands in T1-w images, located around the middle of the cortical thickness (red dotted lines on graphs), were found in calcarine and extra-calcarine cortex for all participants.

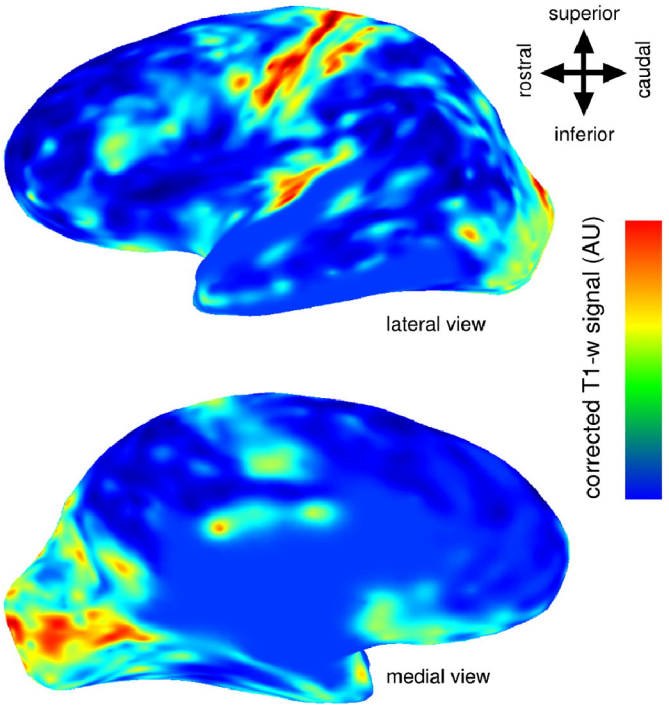

Fig. 7. T1-w intensity across the inflated cortical surface. Inflated pial surfaces were generated using Freesurfer (http://freesurfer.net/) using proton density corrected, T1-w whole-brain scans, sampling halfway the cortical thickness, based on the FreeSurfer cortical thickness estimate. The maps show a number of cortical areas with increased T1-w intensity with respect to the mean. These probable myelination increases are located mainly in primary sensory and motor cortices: Primary visual cortex (calcarine sulcus), primary sensorimotor cortex (central and post-central sulcus), primary auditory cortex (superior temporal sulcus; Heschl's gyrus), and middle temporal cortex (MT+).

($F(3,12) = 8.45$, $p < 0.05$). Statistical analyses reveal that the amplitude of the hypo-intense band in occipital locations was larger than in parietal locations (paired sample t-test, $T(19) = 3.21$, $p < 0.01$, corrected for multiple comparison), frontal locations (paired sample t-test, $T(19) = 3.84$, $p < 0.05$, corrected for multiple comparison), and control locations inside WM (Fig. 10, two sample t-test, $T(28) = 3.74$, $p < 0.01$). When present, the hypo-intense band in WM was 70% smaller than the hypo-intense band inside GM (Fig. 10).

For two participants, we compared the profiles derived at 0.5 mm isotropic with profiles derived at 0.6 mm isotropic from the same locations. Neither the location with respect to cortical thickness nor the amplitude of the T1-w hypo-intense band differed between the profiles obtained for the two acquisitions (paired samples t-test, $t(7) = 0.04$, $p > 0.05$, and $t(7) = 1.85$, $p > 0.05$, respectively), see Fig. 11.

To assess whether within-scan motion corrupted the image quality, we compared the noise level estimates along the phase encoding direction. Noise estimates from the posterior portion of the scan did not differ from estimates derived from the anterior portion of the brain ($t(4) < 1$, $p = 0.29$, ns), indicating that within-scan motion did not corrupt image quality.

Discussion

Summary

We compared laminar profiles from ex vivo T1-w MRI scans to corresponding myelin stained histological samples from the same areas of the human cerebral cortex. Laminar analysis of histology sections revealed a myelin intensity variation located around the middle of the cortical thickness for locations within and outside the calcarine cortex. These profiles mimicked closely the profiles obtained for ex vivo T1-w images, showing a consistent hypo-intense band around the middle of the cortical thickness for both calcarine and extra-calcarine areas of the cortex. Comparable profiles were also obtained for in vivo T1-w images in healthy adults, showing a similar hypo-intense band in T1-w images around the middle of the cortical thickness for both calcarine and extra-calcarine areas. In T1-w images at the level of calcarine cortex, the profile revealed the stria of Gennari. In extra-calcarine cortex, a similar profile was observed, which we suggest corresponds to the lines of Baillarger.

Lines of Baillarger

The lines of Baillarger consist of two bundles of myelinated fibers, located in the internal granular layer of layer IV and internal pyramidal layer of layer V. The laminar profiles extracted from the myelin stained samples did not show a clear demarcation of the two lines of Baillarger. This could be explained by variations in myelin density across the occipital lobe. Histological studies of myelin density across the occipital lobe have shown that myelin distribution and appearance differs between different portions of the samples, and the separate lines of Baillarger (inner and outer) could be identified in some, but not all locations of extra-calcarine areas (Annese et al., 2004; Lungwitz, 1937). For example Annese et al. (2004) studied myelin stains of visual cortex, deriving average intensity profiles for early visual areas. Their data show a clear stria of Gennari in primary visual cortex and a lack of separation between the lines of Baillarger in secondary visual cortex (V2). An extra-calcarine area known for its high myelination is area V3, (Van Essen et al., 1986). In this particular location, it has been shown that the inner and the outer lines of Baillarger are merged, making the distinction between the two impossible. The location of the dorsal portion of this area with respect to the calcarine cortex is compatible with the extra-calcarine area analyzed from the in vivo data of the occipital T1-w scan.

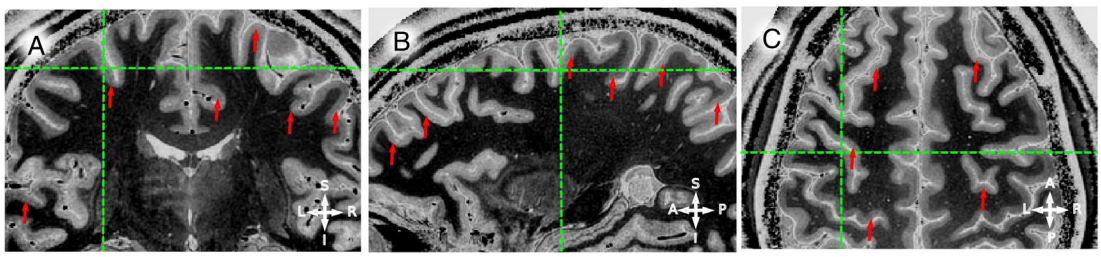

Fig. 8. In vivo whole-brain T1-w data, example coronal, sagittal (panel B), and axial (panel C) slices for one participant (P2, data from the other 4 participants can be found in Fracasso et al., 2016, figures 6-15). Red arrows point to representative locations where an hypo-intense band around the middle of cortical thickness is visible. Green lines mark a corresponding coordinate on the three views. Note that the hypo-intense band can be identified on either hemisphere and from posterior to anterior locations.

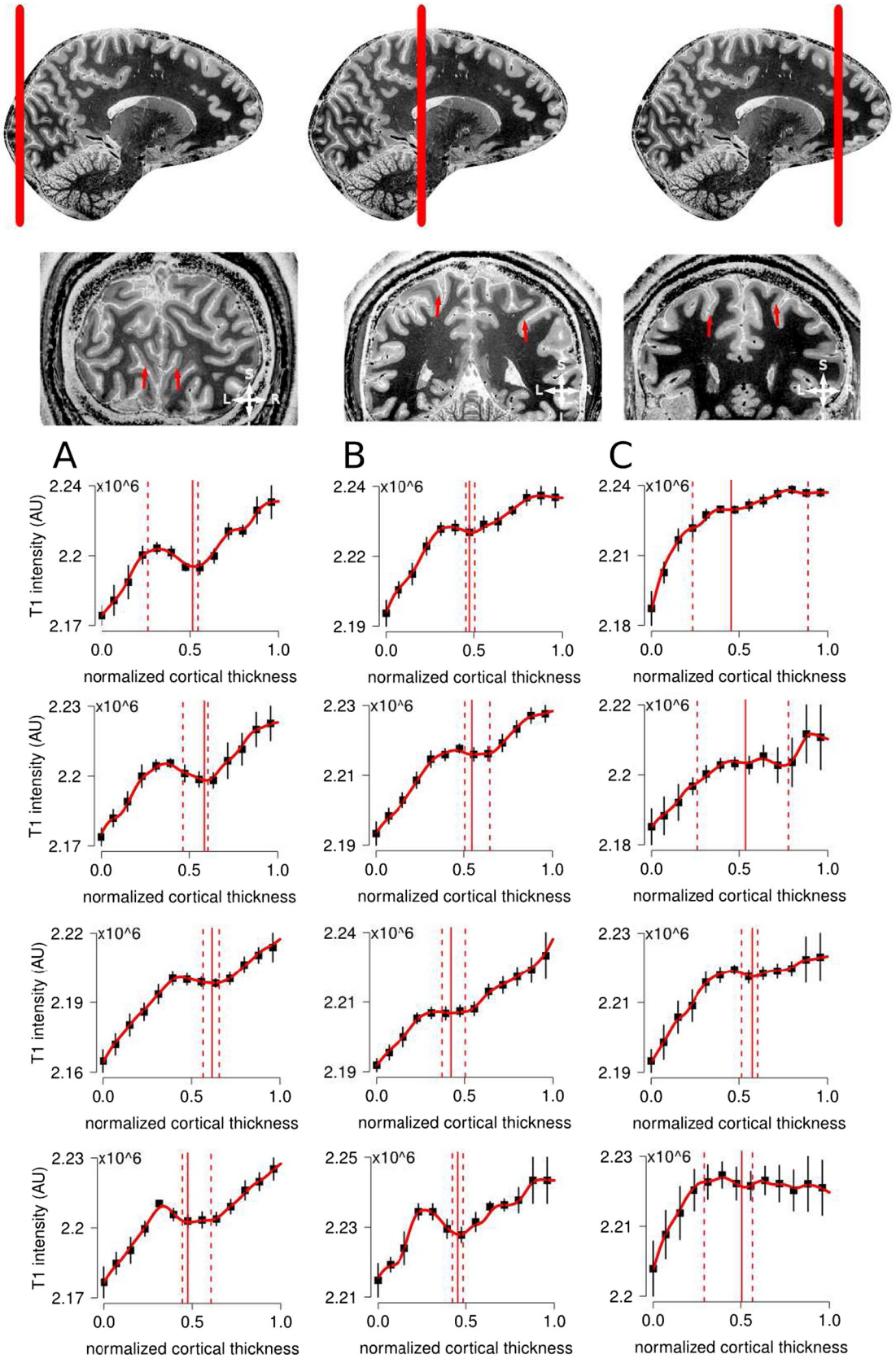

Fig. 9. In vivo whole-brain T1-w data for one participant (P2). Columns correspond to the occipital (A), parietal (B), and frontal (C) lobes as marked by the vertical red line in the sagittal view. Profiles are taken from similar locations in the left and right hemispheres (exemplar locations are marked with red arrows on the corresponding coronal slices). Laminar profiles are reported from the GM/WM border (0 on the x-axis) to the GM/CSF surface (1 on the x-axis) for each location. Error bars indicate standard deviation over all profiles for each location, vertical red lines in graphs represent median and bootstrapped 95% CI of hypo-intense band location. an hypo-intense band in T1-w intensity located around the middle of cortical thickness was identified for all locations (red dashed lines in graphs).

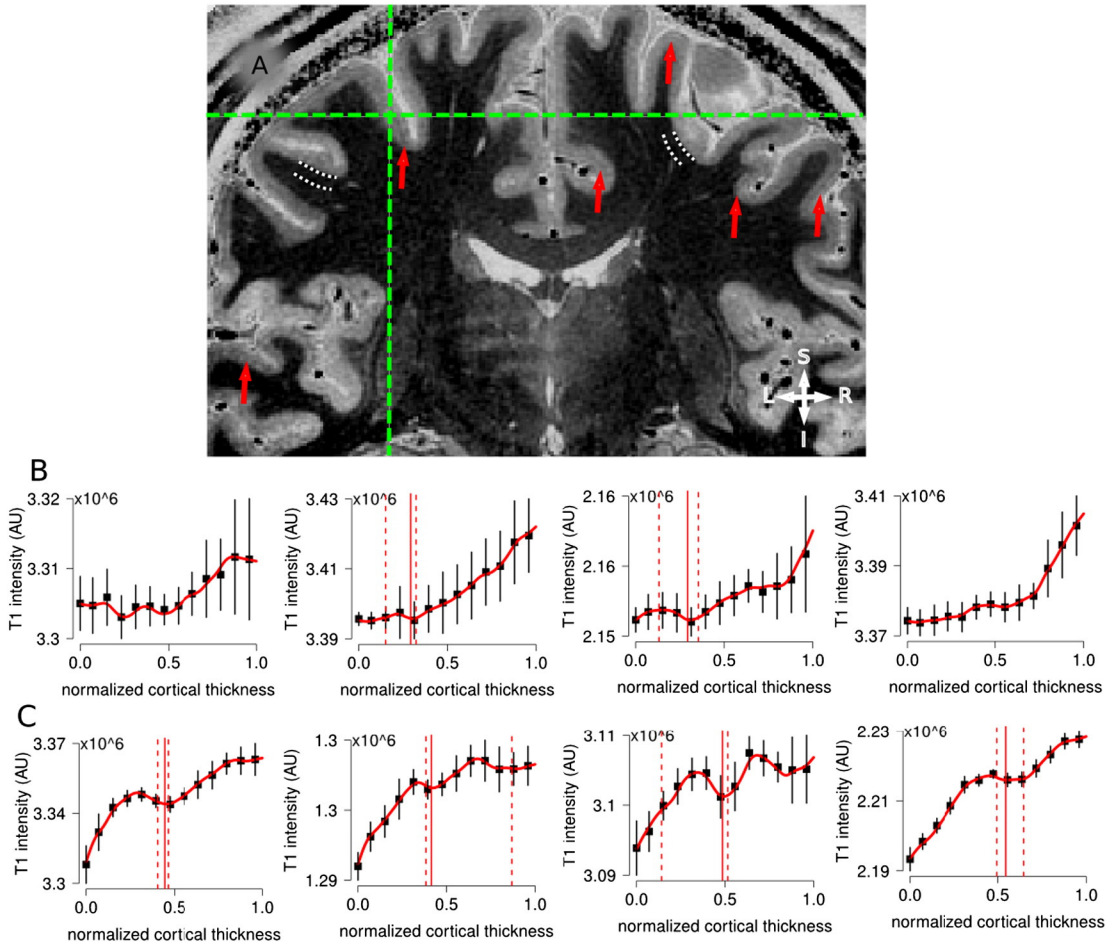

Fig. 10. Panel A, In vivo whole-brain T1-w data, example coronal view. Black and white dotted lines delineate control locations where intensity profiles were extracted inside WM until reaching GM. Red arrows point to locations where a hypo-intense band around the middle of cortical thickness is visible. Row B, T1-w intensity profiles taken from the WM towards the GM border, as depicted in black and white dotted lines in panel A. Row C T1-w intensity profiles taken from the GM towards the CSF border. Error bars indicate standard deviation over all profiles for each location. Sampling intensity profiles inside WM does not yield a similar pattern as that we observe inside GM. A T1-w hypo-intense band was detected on two out of four derived profiles (see profiles in Row B, with and without solid red vertical lines, indicating the presence or absence of a stable T1-w hypo-intense band along the profile). Analysis show that, when present, a hypo-intense band in profile intensity inside WM is about 70% smaller than the one we observe inside GM. If the hypo-intense band that we observe inside GM (see Row C, solid red lines) was due only to Gibbs ringing, then it would manifest on either side of the high contrast GM border, hence inside GM and inside WM, but this is not the case.

We reliably identified a T1-w hypo-intense band located in the middle of the cortical thickness that extended beyond primary visual cortex in both ex vivo and in vivo images. For extra-calcarine locations of the brain, we propose that this structure likely represents the lines of Baillarger (Baillarger, 1840). The two lines of Baillarger could not be separated into the distinctive components. This could be ascribed to a variation in the appearance of the lines of Baillarger in different portions of the occipital lobe (Annese et al., 2004) or that the two lines cannot be separated at the available acquisition resolutions (ex vivo: 0.4 mm isotropic; in vivo: 0.5 mm isotropic).

It is important to remark that the presence and the type of myelin fibers within gray matter formed the basis for the distinctions of qualitative myeloarchitectonics proposed by Vogt (1903; for a recent review, see Geyer and Turner, 2013; Nieuwenhuys, 2013) who described multiple different types of fiber organization in the gray matter. The maps from the Vogt school are based on the combination between the appearance of myelination tangential to the cortical surface (such as the lines of Baillarger), and the myelination radial to cortical surface (Nieuwenhuys, 2013). At the present time, with the resolution available with in vivo MRI, the myelinated fibers extending radially from white matter to gray matter are not directly visible, though the presence of these features might be related to T1-w signal intensity close to the WM border and clustering approaches may help in extracting these type of features (De Martino et al., 2015). However, being able to detect the lines of Baillarger is a first step towards applying the principles of myeloarchitectonics, in vivo, in humans.

Limitations: in vivo data acquisition, motion artifacts and Gibbs ringing

The hypo-intense band located in the middle of cortical thickness (the putative lines of Baillarger) was detected in participants that were familiar with the MRI environment, resulting in minimal motion artifacts. Motion poses a lower limit on the level of detail that can be resolved with high resolution imaging. The use of modern techniques such as prospective motion correction (Qin et al., 2009) to minimize motion artifacts, should help reduce this problem, which constitutes a clear burden, especially for the clinical usage of sub-millimeter resolution MRI.

The Gibbs artifact is usually present where high contrast transitions occur in the image and consists of multiple, parallel bands of alternating bright and dark signal extending from the high contrast border. This particular artifact is caused by k-space truncation. The hypo-intense band that we observe could be partially affected by such an artifact, since it is located closely to a high contrast transition between GM and WM, and GM and CSF.

The hypo-intense band in gray matter did not appear to be coupled with other parallel bands. Instead, a single uniform signal appeared to be present, on coronal, axial, and sagittal slices for the occipital scans

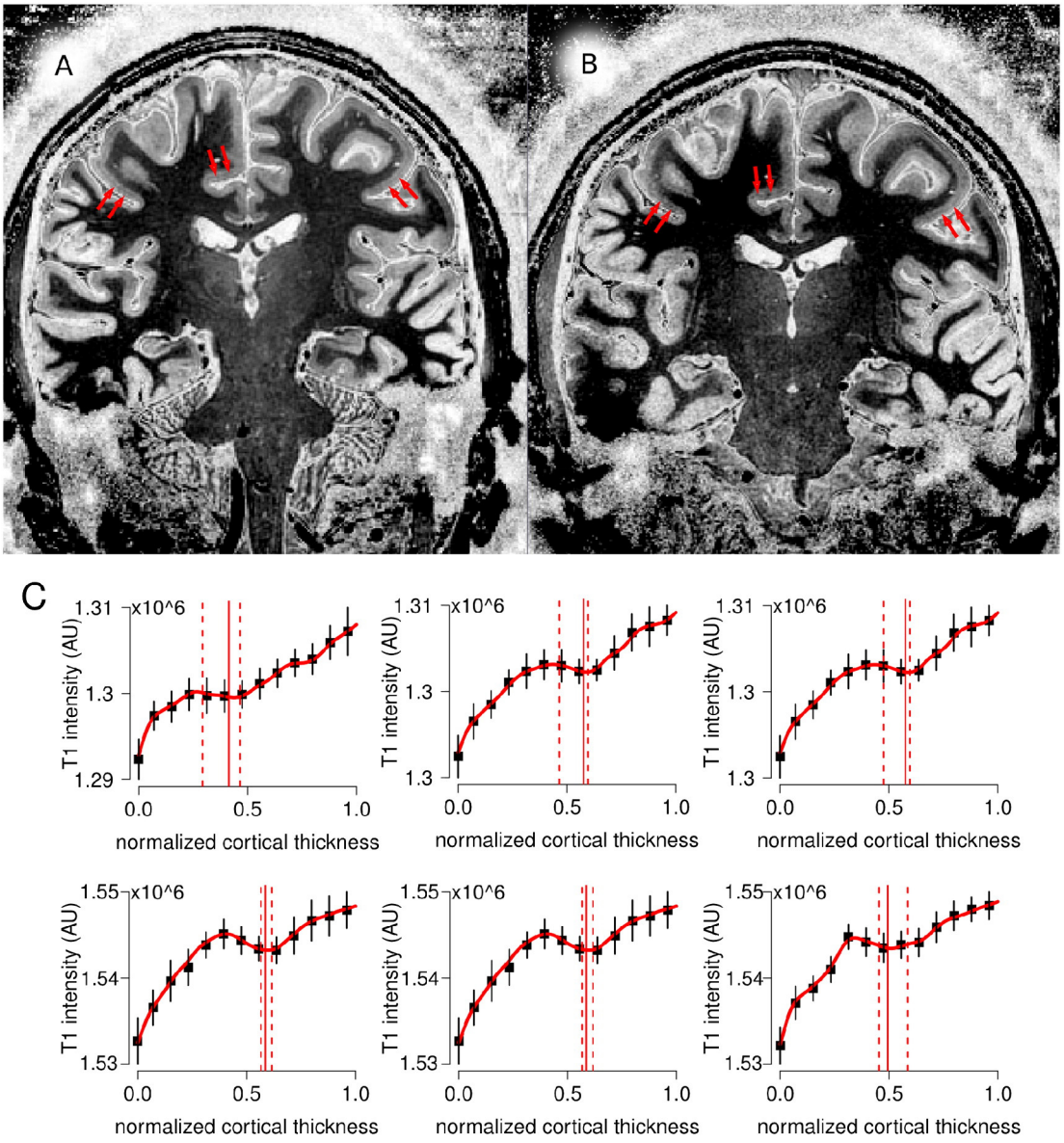

Fig. 11. Panel A, Coronal slices from the T1-w data that was acquired at 0.6 mm. Panel B, Coronal slice from the T1-w data acquired at 0.5 mm for the same participant (similar slice location as in panel A). Row C: T1-w intensity profiles derived at 0.6 mm isotropic. Row D: T1-w intensity profiles derived at 0.5 mm isotropic from similar locations as row C. Red arrows point to locations where the profiles were extracted. Neither the location with respect to cortical thickness nor the amplitude of the T1-w hypo-intense band differed between the profiles obtained for the two acquisitions (paired samples t-test, $t(7) = 0.04$, $p > 0.05$ and $t(7) = 1.85$, $p > 0.05$, respectively). Profiles are very similar for the two acquisitions. If truncation artifacts were affecting the results in the analyzed locations, we would expect the intra-cortical feature to shift position by changing the acquisition resolution.

(see Fig. 5C and Fracasso et al., 2016, Figures 2–5) and whole-brain scans (see Fig. 8 and Fracasso et al., 2016, Figures 6–15). This pattern is not consistent with the Gibbs artifact.

The Gibbs artifact would manifest on either side of a high contrast border (inside GM but and also inside WM). Sampling intensity profiles inside WM did not yield a consistent hypo-intense band as that we observed inside GM (Fig. 10). Analysis showed that, when present, the amplitude of the hypo-intense band in the profile intensity inside WM was about 70% smaller than what was observed inside GM (Fig. 10).

The same whole-brain sequence was used to acquire additional data for two participants with a different resolution (0.6 mm, isotropic) with all other parameters being the same. The profiles derived from the same locations were virtually indistinguishable from those derived at 0.5 mm (Fig. 11). If truncation artifacts were affecting the results we would have expected the hypo-intense band to shift position by changing the acquisition resolution.

To summarize, the Gibbs artifact is a serious concern for laminar MRI, given the presence of high contrast borders in the close proximity of GM, but it is very unlikely that the hypo-intense band that we report in this manuscript reflects only the contribution of Gibbs ringing inside GM.

Myelin and iron content

T1-w contrast broadly reflects differences in lipid concentration (Koenig, 1991) that are tied to myelin, but is also strongly influenced by iron content (Fukunaga et al., 2010; Stueber et al., 2014). Iron content strongly contributes to the contrast observed in T2*-w images as well. One of the main origins of T2*-w contrast is the magnetic susceptibility of lipid molecules, especially those containing iron, such as ferritin (Duyn, 2011; Duyn et al., 2007). These molecules are present in particularly high concentration especially in the blood as well as white matter,

in correspondence with the myelin sheet that surrounds the axons to facilitate the propagation of impulses along their length. Thus it is likely that our T1-w contrast reflects a combination of iron and myelin localized in the gray matter.

T2-w signal amplitude and phase*

T2*-w profiles did not show a consistent hypo-intense band in T1-w images around the middle of the cortical thickness on extra-calcarine locations for the ex vivo sample. We limited our profile analysis to the amplitude of the T2*-w signal. It has been shown that, at high magnetic field strength, the phase of the T2*-w signal shows dramatic improvements in SNR (Duyn et al., 2007). It is thus possible that the phase of the T2*-w signal would be more sensitive to laminar myelin variations than the amplitude alone. For this reason we cannot exclude that T2*-w images might show a significant hypo-intense band, located around the middle of the cortical thickness outside the calcarine cortex, for profiles obtained using the phase of the T2*-w signal.

Quantitative imaging

Here we adapted a T1-w MPRAGE sequence to visualize the lines of Baillarger, thus report T1-w intensity profiles. The sequence could be expanded to include additional readouts with different TIs, for instance similar to a T1-w MP2RAGE (Marques and Gruetter, 2013) to allow for quantitative T1 estimation (Stueber et al., 2014; Dinse et al., 2015). Quantitative T1 imaging can be beneficial when comparing across subjects and different scanners, as it is less susceptible to B1 and receive field inhomogeneities. We show, however, that the ability to visualize the lines of Baillarger does not depend on quantitative imaging. Using this sequence, we observe a robust hypo-intense band around the middle of the cortical thickness for both calcarine and extra-calcarine areas of the cortex. The amplitude of the hypo-intense band was larger in the calcarine than on extra-calcarine locations ($\mu = 13.4\%$ $\sigma = \pm 3.9$ and $\mu = 9.1\%$, $\sigma = \pm 5.5$, respectively), as could be expected from histology literature (Geyer and Turner, 2013; Nieuwenhuys, 2013). Another interesting observation is the clear reversed contrast at the level of the CSF (see Figs. 5,6 and 8) which may provide a better way to define the pial boundary for automatic segmentation algorithms.

Conclusions

In the present study, we showed very high spatial resolution T1-w images of ex vivo and in vivo data at 7 T. A hypo-intense band located in the middle of the cortex was identified in calcarine cortex as well as in extra-calcarine areas on T1-w intensity profiles. This structure was found in cortical areas well outside the calcarine cortex, for example frontal cortex, a region typically not associated with increased myelination. We suggest that this structure represents the two lines of Baillarger. We show that it is possible to identify well-defined hypo-intense bands, inside GM, not only within primary visual cortex (stria of Gennari) but also outside the calcarine cortex in parietal and frontal lobes.

Acknowledgments

This work was supported by a Netherlands Organization for Scientific Research (NWO) Vidi Grant 452-08-008 (S.O.D.) and 13339 (N.P.), and by the European Research Council under the European Union's Seventh Framework Program (FP7/2007-2013) / ERC grant agreement no. 337333 (J.J.M.Z.).

Conflict of interest

None.

References

Annese, J., Pitiot, A., Dinov, I.D., Toga, A.W., 2004. A myelo-architectonic method for the structural classification of cortical areas. NeuroImage 21, 15–26.
Baillarger, J., 1840. Recherces sur la structure de la couche corticale des circonvolutions du cerveau. Mem. Acad. R. Med. 8.
Barbier, E.L., Marrett, S., Danek, A., Vortmeyer, A., van Gelderen, P., Duyn, J., Bandettini, P., Grafman, J., Koretsky, A.P., 2002. Imaging cortical anatomy by high-resolution MR at 3.0 T: detection of the stripe of Gennari in visual area 17. Magn. Reson. Med. 48, 735–738. http://dx.doi.org/10.1002/mrm.10255.
Bock, N.A., Kocharyan, A., Liu, J.V., Silva, A.C., 2009. Visualizing the entire cortical myrelination pattern in marmosets with magnetic resonance imaging. J. Neurosci. Methods 185, 15–22. http://dx.doi.org/10.1016/j.jneumeth.2009.08.022.
Bock, N.A., Hashim, E., Janik, R., Konyer, N.B., Weiss, M., Stanisz, G.J., Turner, R., Geyer, S., 2013. Optimizing T(1)-weighted imaging of cortical myelin content at 3.0 T. NeuroImage 65, 1–12.
Bridge, H., Clare, S., Jenkinson, M., Jezzard, P., Parker, A.J., Matthews, P.M., 2005. Independent anatomical and functional measures of the V1/V2 boundary in human visual cortex. J. Vis. 5, 93–102. http://dx.doi.org/10.1167/5.2.1.
Brodmann, K., 1909. Vergleichende Lokalisationslehre Der Großhirnrinde. J.A. Barth, Leipzig.
De Martino, F., Moerel, M., Xu, J., van de Moortele, P.F., Ugurbil, K., Goebel, R., Yacoub, E., Formisano, E., 2015. High-resolution mapping of myeloarchitecture in vivo: localization of auditory areas in the human brain. Cereb. Cortex 25 (10), 3394–3405.
Dinse, J., Härtwich, N., Waehnert, M.D., Tardif, C.L., Schäfer, A., Geyer, S., Preim, B., Turner, R., Bazin, P.L., 2015. A cytoarchitecture-driven myelin model reveals area-specific signatures in human primary and secondary areas using ultra-high resolution in-vivo brain MRI. Neuroimage 114, 71–87 (Jul 1).
Duyn, J.H., 2011. High-field MRI of brain iron. Methods Mol. Biol. 711, 239–249. http://dx.doi.org/10.1007/978-1-61737-992-5_11.
Duyn, J.H., van Gelderen, P., Li, T.-Q., de Zwart, J.A., Koretsky, A.P., Fukunaga, M., 2007. High-field MRI of brain cortical substructure based on signal phase. Proc. Natl. Acad. Sci. U. S. A. 104, 11796–11801. http://dx.doi.org/10.1073/pnas.0610821104.
Eickhoff, S., Walters, N.B., Schleicher, A., Kril, J., Egan, G.F., Zilles, K., Watson, John D.G., Amunts, K., 2005. High-resolution MRI reflects myeloarchitecture and cytoarchitecture of human cerebral cortex. Hum. Brain Mapp. 24 (3), 206–215.
Fedorov, A., Beichel, R., Kalpathy-Cramer, J., Finet, J., Fillion-Robin, J.-C., Pujol, S., Bauer, C., Jennings, D., Fennessy, F., Sonka, M., Buatti, J., Aylward, S., Miller, J.V., Pieper, S., Kikinis, R., 2012. 3D slicer as an image computing platform for the quantitative imaging network. Magn. Reson. Imaging 30, 1323–1341. http://dx.doi.org/10.1016/j.mri.2012.05.001.
Fischl, B., Rajendran, N., Busa, E., Augustinack, J., Hinds, O., Yeo, B.T.T., Mohlberg, H., Amunts, K., Zilles, K., 2008. Cortical folding patterns and predicting cytoarchitecture. Cereb. Cortex 18, 1973–1980. http://dx.doi.org/10.1093/cercor/bhm225.
Fracasso, A., van Veluw, S.J., Visser, F., Luijten, P., Spliet, W., Zwanenburg, J.J., Dumoulin, S.O., Petridou, N., 2016. Myelin contrast across lamina at 7 T. Data Brief.
Fukunaga, M., Li, T.-Q., van Gelderen, P., de Zwart, J.A., Shmueli, K., Yao, B., Lee, J., Maric, D., Aronova, M.A., Zhang, G., Leapman, R.D., Schenck, J.F., Merkle, H., Duyn, J.H., 2010. Layer-specific variation of iron content in cerebral cortex as a source of MRI contrast. Proc. Natl. Acad. Sci. U. S. A. 107, 3834–3839. http://dx.doi.org/10.1073/pnas.0911177107.
Gennari, F., 1782. De Peculiari Structura Cerebri. Nonnullisque ejus morbis. Ex Regio Typographeo, Parma.
Geyer, S., Turner, R., 2013. Microstructural Parcellation of the Human Cerebral Cortex. Springer, London.
Glasser, M.F., Van Essen, D.C., 2011. Mapping human cortical areas in vivo based on myelin content as revealed by T1- and T2-weighted MRI. J. Neurosci. 31, 11597–11616. http://dx.doi.org/10.1523/JNEUROSCI.2180-11.2011.
Hinds, O.P., Rajendran, N., Polimeni, J.R., Augustinack, J.C., Wiggins, G., Wald, L.L., Rosas, H.D., Potthast, A., Schwartz, E.L., Fischl, B., 2008. Accurate prediction of V1 location from cortical folds in a surface coordinate system. NeuroImage 39, 1585–1599. http://dx.doi.org/10.1016/j.neuroimage.2007.10.033.
Koenig, S., 1991. Cholesterol of myelin is the determinant of gray-white contrast in mri. Magn. Reson. Med. 20, 285–291. http://dx.doi.org/10.1002/mrm.1910200210.
Lungwitz, W., 1937. Zur myeloarchitektonischen Untergliederung der menschlichen Area praeoccipitalis (Area 19 Brodmann). J. Psychol. Neurol. 47, 607–639.
Lutti, A., Dick, F., Sereno, M.I., Weiskopf, N., 2014. Using high-resolution quantitative mapping of R1 as an index of cortical myelination. NeuroImage 93 (Pt 2), 176–188. http://dx.doi.org/10.1016/j.neuroimage.2013.06.005.
Marques, J.P., Gruetter, R., 2013. New developments and applications of the MP2RAGE sequence-focusing the contrast and high spatial resolution R1 mapping. PLoS One 8 (7), e69294.
Nieuwenhuys, R., 2013. The myeloarchitectonic studies on the human cerebral cortex of the Vogt–Vogt school, and their significance for the interpretation of functional neuroimaging data. Brain Struct. Funct. 218, 303–352. http://dx.doi.org/10.1007/s00429-012-0460-z.
Nieuwenhuys, R., Broere, C.A., Cerliani, L., 2014. A new myeloarchitectonic map of the human neocortex based on data from the Vogt–Vogt school. Brain Struct. Funct. 220, 2551–2573. http://dx.doi.org/10.1007/s00429-014-0806-9.
Qin, L., van Gelderen, P., Derbyshire, J.A., Jin, F., Lee, J., de Zwart, J.A., Tao, Y., Duyn, J.H., 2009. Prospective head-movement correction for high-resolution MRI using an in-bore optical tracking system. Magn. Reson. Med. 62, 924–934. http://dx.doi.org/10.1002/mrm.22076.
Ress, D., Glover, G.H., Liu, J., Wandell, B., 2007. Laminar profiles of functional activity in the human brain. NeuroImage 34, 74–84. http://dx.doi.org/10.1016/j.neuroimage.2006.08.020.

Sánchez-Panchuelo, R.M., Francis, S.T., Schluppeck, D., Bowtell, R.W., 2012. Correspondence of human visual areas identified using functional and anatomical MRI in vivo at 7 T. J. Magn. Reson. Imaging 35, 287–299. http://dx.doi.org/10.1002/jmri.22822.

Sánchez-Panchuelo, R.M., Besle, J., Mougin, O., Gowland, P., Bowtell, R., Schluppeck, D., Francis, S., 2014. Regional structural differences across functionally parcellated brodmann areas of human primary somatosensory cortex. NeuroImage 93, 221–230.

Sereno, M.I., Lutti, A., Weiskopf, N., Dick, F., 2013. Mapping the human cortical surface by combining quantitative T(1) with retinotopy. Cereb. Cortex 1991 (23), 2261–2268. http://dx.doi.org/10.1093/cercor/bhs213.

Stueber, C., Morawski, M., Schaefer, A., Labadie, C., Waehnert, M., Leuze, C., Streicher, M., Barapatre, N., Reimann, K., Geyer, S., Spemann, D., Turner, R., 2014. Myelin and iron concentration in the human brain: a quantitative study of MRI contrast. NeuroImage 93, 95–106. http://dx.doi.org/10.1016/j.neuroimage.2014.02.026.

Tardif, C.L., Schäfer, A., Waehnert, M., Dinse, J., Turner, R., Bazin, P.-L., 2015. Multi-contrast multi-scale surface registration for improved alignment of cortical areas. NeuroImage 111, 107–122. http://dx.doi.org/10.1016/j.neuroimage.2015.02.005.

Trampel, R., Ott, D.V.M., Turner, R., 2011. Do the congenitally blind have a stria of Gennari? First intracortical insights in vivo. Cereb. Cortex 1991 (21), 2075–2081. http://dx.doi.org/10.1093/cercor/bhq282.

Van Essen, D.C., Newsome, W.T., Maunsell, J.H., Bixby, J.L., 1986. The projections from striate cortex (V1) to areas V2 and V3 in the macaque monkey: asymmetries, areal boundaries, and patchy connections. J. Comp. Neurol. 244, 451–480. http://dx.doi.org/10.1002/cne.902440405.

Vogt, O., 1903. Zur anatomischen Gliederung des Cortex cerebri. J. Psychol. Neurol. 2, 160–180.

von Economo, C., Koskinas, G.N., 1925. Die Cytoarchitektonik der Hirnrinde des Erwachsenen Menschen: Textband und Atlas mit 112 Mikrophotographischen Tafeln. Springer, Vienna.

Waehnert, M.D., Dinse, J., Weiß, M., Streicher, M.N., Waehnert, P., Geyer, S., ... Bazin, P.L., 2014. Anatomically motivated modeling of cortical laminae. NeuroImage 93, 210–220.

Walters, N.B., Egan, G.F., Kril, J.J., Kean, M., Waley, P., Jenkinson, M., Watson, J.D., 2003. In vivo identification of human cortical areas using high-resolution MRI: an approach to cerebral structure–function correlation. Proc. Natl. Acad. Sci. 100 (5), 2981–2986.